Current Cardiovascular Imaging Reports (2019) 12: 28
https://doi.org/10.1007/s12410-019-9501-9

MOLECULAR IMAGING (J WU AND P NGUYEN, SECTION EDITORS)

# Nanoparticle Imaging of Vascular Inflammation and Remodeling in Atherosclerotic Disease

Darren G. Woodside[1]

Published online: 29 May 2019


## Abstract

**Purpose of Review** The purpose of this review is to highlight some of the recent developments (within the last 5 years) in imaging atherosclerotic plaques using nanoparticles, with a focus on technologies that have been applied to in vivo models of disease.

**Recent Findings** Structural and cellular components of atherosclerotic plaques are being imaged with greater definition and improved sensitivity. This is a result of both molecular targeting of nanoparticles to disease-relevant biomarkers through the use of nanoparticles of different shapes and sizes and tailoring pharmacokinetic parameters that allow for enhanced pharmacodynamic effects.

**Summary** Currently, there are no atherosclerotic plaque imaging techniques clinically validated to predict future clinical events. Considering the rapid pace of new nanomaterial discovery and development, along with the development of multimodality imaging systems, this goal seems within reach. These advancements are "nano" in name only.

**Keywords** Atherosclerosis · Inflammation · Nanoparticles · Imaging · Plaques · Leukocytes

## Introduction

According to statistics gathered by the World Health Organization, cardiovascular disease (CVD) has been the single leading cause of death worldwide for the past 15 years [1]. In 2016 alone, greater than 15 million deaths were reported to be caused by ischemic heart disease and stroke [1]. An underling cause of CVD is atherosclerosis. Atherosclerosis is a chronic inflammatory disease of small-to-medium-sized arteries that can cause luminal narrowing and reduced blood flow or acute ischemic events (like myocardial infarction or stroke) due to inflammatory foci rupture or erosion. As such, the development of novel technologies to image the generation and progression of atherosclerotic plaques or to monitor the effectiveness of treatment strategies could have a significant effect on the treatments used and the course of CVD. This review describes the progress made in the last 5 years to develop nanoparticle-based techniques for in vivo imaging of vascular inflammation in patients with atherosclerosis, with particular emphasis on imaging the structural and cellular elements of plaques. Additional reviews of imaging approaches for atherosclerosis can be found elsewhere, including one on current clinical and preclinical approaches to molecular positron emission tomography (PET) imaging by Vigne et al. [2] and a general compendium of recently described nanoprobes for in vivo imaging [3].

## Atherosclerosis

The Canakinumab Anti-inflammatory Thrombosis Outcomes Study (CANTOS) demonstrated that neutralizing the pro-inflammatory cytokine IL-1β with a selective monoclonal antibody (mAb) could prevent major cardiac adverse events independent of lipid lowering [4]. This is considered definitive clinical evidence in support of the inflammatory hypothesis of atherosclerosis [5]. Atherosclerosis is driven by the immune system's responses to the accumulation of low-density lipoprotein (LDL) cholesterol in small-to-medium arteries. The pathobiology is well described from clinical observations and animal models, which have led to the identification of numerous features that can be targeted for imaging purposes (Fig. 1).

This article is part of the Topical Collection on *Molecular Imaging*

✉ Darren G. Woodside
DWoodside@texasheart.org

[1] Department of Molecular Cardiology, Texas Heart Institute, 6770 Bertner Avenue, MC 2-255, Houston, TX 77030, USA

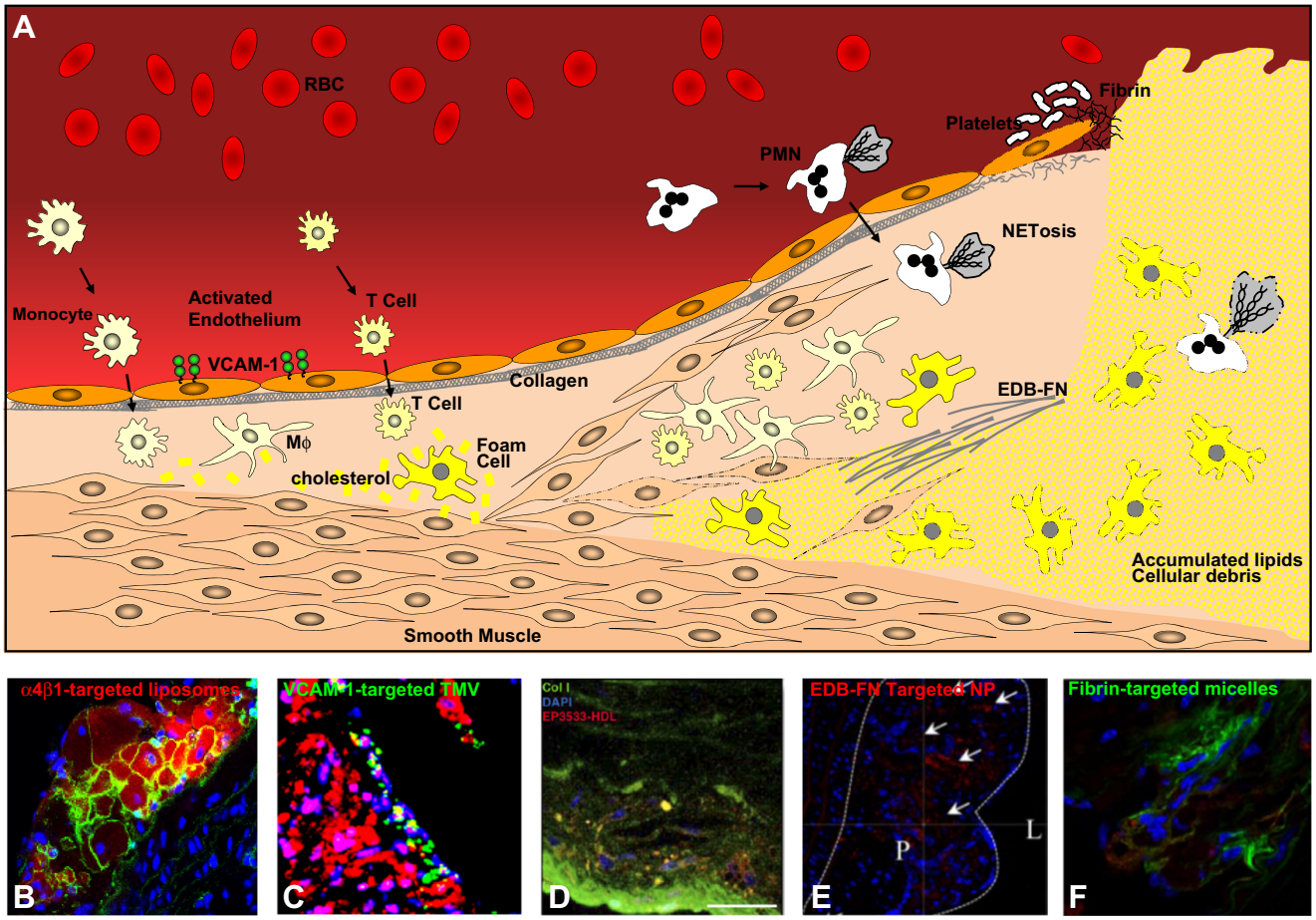


**Fig. 1** Recent nanoparticle-based approaches targeting cellular and structural components of atherosclerotic plaques for imaging. **a** Simplistic view of some of the structural and cellular elements in an unstable plaque. For clarity, soluble inflammatory mediators are not shown. **b** Integrin α4β1-targeted liposome accumulation in inflammatory cells in plaques of ApoE$^{-/-}$ mice. Adapted from Woodside et al. [6] with permission. **c** VCAM-1-targeted tobacco mosaic virus (TMV) lining plaque endothelial cells in ApoE$^{-/-}$ mice. Adapted with permission from Bruckman et al. [7]. **d** Accumulation of collagen-targeted high-density lipoproteins (EP3533-HDL) in healing atherosclerotic plaques in the Reversa model of atherosclerosis regression. Adapted from Chen et al. [8] with permission. **e** Nanoparticles targeted to the alternatively spliced ENB isoform of fibronectin (EDB-FN targeted NP) within the central core region of plaques in ApoE$^{-/-}$ mice. P, plaque; L, lumen. Adapted from Yu et al. [9] with permission. **f** Fibrin-targeted micelles in ApoE$^{-/-}$ mice. Adapted from Peters et al. [10] with permission. Col I, collagen type I; DAPI, 4′,6-diamidino-2-phenylindole; EDB-FN, extra domain B of fibronectin; Mφ, macrophage; NET, neutrophil extracellular trap; PMN, polymorphonuclear leukocyte; RBC, red blood cell; VCAM-1, vascular cell adhesion molecule-1

Atherosclerosis, a non-resolving inflammation, begins in small-to-medium-sized arteries at sites of disturbed blood flow, where lipoproteins like cholesterol-enriched LDL accumulate within subendothelial compartments. Accumulation can occur through increased endothelial cell permeability and paracellular transport or through receptor-mediated transcytosis [11]. The accumulated lipoproteins undergo modifications like oxidation and aggregation [11], which facilitates their engulfment by innate immune cells. These cells, such as tissue-resident vascular macrophages, recognize these lipid deposits through pattern recognition receptors and scavenger receptors like CD36 [12]. Binding and internalization of oxidized LDL and lipoprotein deposits proceed without regulation, leading to intracellular accumulation and nucleation of cholesterol crystals, which ultimately results in activation of the NLRP3 inflammasome [11]. A major outcome of inflammasome activation is the production of pro-inflammatory cytokines like IL-1β, which can induce local effects such as smooth muscle and endothelial cell activation and the production of IL-6 and PGE2, which can have systemic effects [13]. Endothelial cell activation and upregulation of adhesion molecules like vascular cell adhesion molecule-1 (VCAM-1) work in concert with chemokines to recruit immune cells like monocytes and T cells [14–16]. Cellular recruitment to plaques is an ongoing process that begins in the nascent phase of plaque initiation and persists through plaque development. The overall cellularity of an atherosclerotic plaque depends on cellular recruitment from both the vessel lumen and vaso vasorum and subsequent cellular proliferation and apoptosis; this process can result in an array of immune cells suggestive of tertiary lymphoid tissue [17]. Toll-like receptors can also bind

modified LDL in the subendothelial space, which can result in the production of inflammatory mediators, like tumor necrosis factor (TNF), that regulate matrix metalloproteinase expression, thereby influencing tissue remodeling. Tissue resident dendritic cells can capture modified LDLs, migrate to lymph nodes that drain the atherosclerotic plaque, and present modified LDL fragments to antigen-specific T cells. This largely results in the generation TH1-type effector cells, which can recirculate to plaques and become activated by local antigen-presenting cells [13]. T cell production of TNFα and IFNγ further drives macrophage, endothelial cell, and smooth muscle cell activation, which further promotes inflammatory cell recruitment into plaques and can cause deterioration of the structural integrity of the physical "cap" of the plaque by limiting collagen deposition by vascular smooth muscle cells and increasing matrix degradation, at least in the case of traditional plaque rupture [13]. In the case of plaque erosion, polymorphonuclear cell involvement is more prevalent, and the traditional structural characteristics of decreased collagen and smooth muscle cell content are not typically observed [18]. However, the overall consequence of plaque inflammation is the breakdown of the physical barrier covering the plaque, which can result in thrombotic complications.

Many approaches for imaging inflammation in atherosclerotic plaque take advantage of our knowledge about plaque architecture and the pathogenesis of atherosclerosis. These approaches target either the structural components of plaque, like the content of the extracellular matrix (ECM), or the cellular components.

## Structural Elements

Histological examination of culprit plaques in patients who have had a fatal myocardial infarction has indicated that reduced fibrous cap thickness is a contributing factor to both rupture and erosion. Collagens and elastins produced by vascular smooth muscle cells and fibroblasts make up a large portion of the ECM in atherosclerotic plaques, including in the fibrous cap. Structural integrity is maintained by balancing ECM production and degradation; this is done by proteolytic enzymes produced by inflammatory cells. Degradation is the prevailing process in culprit lesions, especially in those that rupture. Most reports about imaging agents specific for the ECM components of plaque describe molecule-based molecular probes for both magnetic resonance (MR) and PET imaging (recently reviewed by Reimann et al. [19]). The relatively few probes that are nanoparticle-based are described below.

### Elastin

Sinha et al. [20] conjugated poly (D,L-lactide) (PLA) nanoparticles loaded with 1,1-dioctadecyl-3,3,3,3-tetramethylindotricarbocyanine iodide (DIR) dye to rabbit polyclonal anti-elastin antibodies and used these nanoparticles to image damaged elastic lamina in injured vessels [20]. When injected into $ApoE^{-/-}$ mice on a high-fat diet, the elastin-targeted nanoparticles localized to sites of atherosclerotic plaque but not to sites with healthy tissue, despite the presence of elastin in healthy tissue. The nanoparticles apparently showed this specificity because the conjugated anti-elastin antibodies only recognized epitopes that were exposed upon elastin cleavage. Unfortunately, in these $ApoE^{-/-}$ mouse experiments, nanoparticles conjugated to non-specific rabbit immunoglobulin (Ig) were not tested as a control, making it difficult to determine the specificity of plaque uptake and the contributions due to engulfment by phagocytic cells.

### Collagen

One of the benefits of targeting ECM components in plaques is the relative abundance of molecular targets. Recently, groups have developed nanoparticles based on mimetics of high-density lipoprotein (HDL) particles [8, 21]. These are in vitro constructs, but they mimic components of endogenous HDLs (containing ApoA-I) and have been used to image plaque contents. Although minimally modified HDL-like particles are primarily taken up through endocytosis by macrophages, HDL-like nanoparticles can be further functionalized to better target plaque by incorporating peptides that specifically bind collagen, such as EP-3533 [22]. EP3533-HDL-like nanoparticles have shown utility in the Reversa model of atherosclerotic plaque regression [8].When these nanoparticles were modified to incorporate Gd and used for MR imaging, the nanoparticles were found to colocalize with collagen in plaques. The same study showed that EP3533-HDL-like nanoparticles could be used to discriminate between various types of ECM components (like collagen and laminin) but not between collagen subtypes I, III, IV, and V. At 28 days after induction of plaque regression in the Reversa model, the MR signal at sites of plaques was significantly enhanced with the EP3533-HDL-like nanoparticles but not with the controls (naked HDL or non-specific control peptide conjugated to HDL-like nanoparticles) (Fig. 2c, d). This enhancement correlated with a decrease in macrophage content and an increase in type I collagen in the regressing plaques. Imaging agents such as this may be helpful when imaging plaques in patients who are undergoing therapeutic interventions for plaque stabilization. Although the Reversa model is an interesting model to study plaque regression, this work will need to be repeated in animal models that are undergoing standard treatments like statin therapies to determine how the imaging agent performs under current therapeutic standards of care.

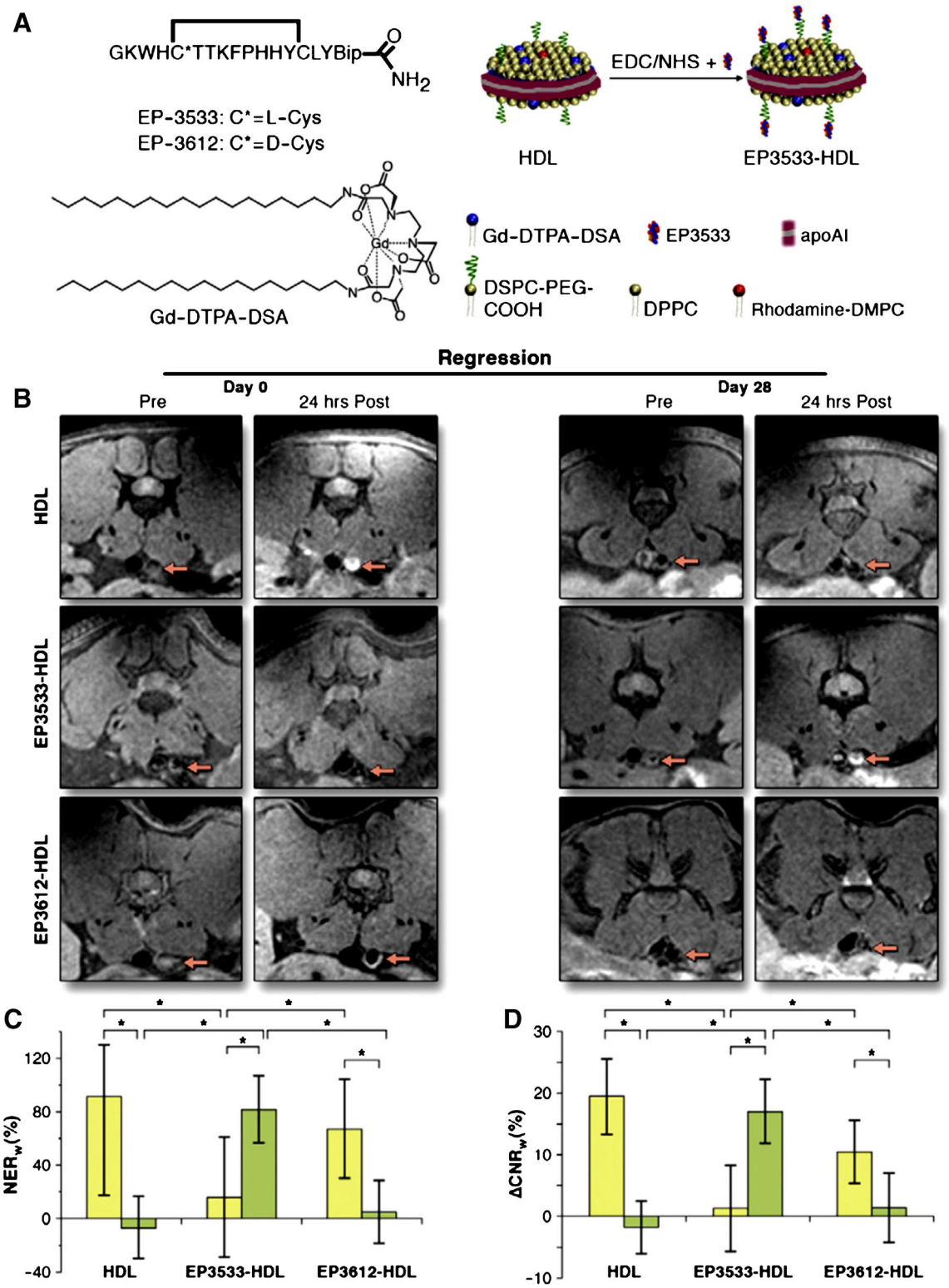


## Fibronectin

The extra domain B of fibronectin (EDB-FN) is an alternative splice variant of fibronectin that is upregulated at sites of tissue remodeling, including sites of tumor angiogenesis [23] and within atherosclerotic plaques [24, 25]. Peptide aptamers that were developed to selectively target EDB-FN [26] were used to generate EDB-FN-specific Gd nanoparticles ($APT_{FN\text{-}EDB}$-[Gd]NP), which were then tested in a murine $ApoE^{-/-}$ model of atherosclerosis [9]. Contrast normalized ratios

◀ **Fig. 2** **a** Method to functionalize high-density lipoprotein (HDL) nanoparticles with collagen-specific EP3553 peptides (EP3533-HDL). **b**–**d** Typical magnetic resonance images (**b**), NERw (**c**), and ΔCNRw (**d**) of abdominal atherosclerotic plaques before and 24 h after injection of HDL, EP3533-HDL, or EP3612-HDL (control peptide) at day 0 (yellow bars) and day 28 (green bars) in Reversa mouse model of plaque regression. The arrows point to the aortas. The error bars represent mean ± SD. The asterisks (*) indicate statistical significance at $P < 0.05$ ($n = 5$ mice × 5 slices/mouse = 25). ApoA-I, apolipoprotein A-I; DPPC, 1,2-dipalmitoyl-sn-glycero-3-phosphocholine; DSPC-PEG-COOH, 1,2-distearoyl-sn-glycero-3-phosphoethanolamine-*N*-[carboxy(polyethylene glycol)-2000] ammonium salt; EDC, 1-ethyl-3-[3-dimethylaminopropyl]carbodiimide hydrochloride; GD-DPTA-DSA, gadolinium diethylenetriaminepentaacetate-bis(stearylamide); NHS, *N*-hydroxysuccinimide; rhodamine-DMPC, 1,2-dimyristoyl-sn-glycero-3-phosphoethanolamine-*N*-(Lissamine rhodamine B sulfonyl); CNR, contrast-to-noise ratio; NER, normalized enhancement ratio; w, aortic vessel wall. Adapted from Chen et al. [8] with permission

between the aortic wall and lumen were significantly higher with $APT_{FN\text{-}EDB}$-[Gd]NPs than with scrambled peptide-targeted control nanoparticles (Fig. 3d–f). Furthermore, free EDB-FN peptide aptamers were able to inhibit the signal generated by $APT_{FN\text{-}EDB}$-[Gd]NPs. Because EDB-FN expression is correlated with advanced stages of atherosclerotic plaques [9], this may be an interesting approach for risk stratifying patients and monitoring the effectiveness of treatment strategies.

### Fibrin

Platelets bind to exposed ECM at sites of endothelial damage along atherosclerotic lesions. Platelet activation and aggregation induce the production of thrombin, which converts fibrinogen to fibrin, resulting in the generation of microthrombi, which can lead to thrombus formation and vessel occlusion. Nanoparticles have been developed that target fibrin through the incorporation of fibrin-binding peptides. These peptides include the cyclic fibrin-binding peptide RWQPCPAESWT-Cha-CWDP and CREKA, both of which were originally identified from phage display libraries [27]. When modified with $^{111}$Ind, RWQPCPAESWT-Cha-CWDP peptides have been shown to accumulate at the sites of fibrin deposition and have been successfully used for molecular imaging of fibrin deposition with single-photon emission computerized tomography (SPECT) [28]. However, when coupled to iron oxide nanoparticle micelles, the peptide-targeting specificity was lost; the control peptide-targeted iron oxide nanoparticle micelles and the target peptide-conjugated nanoparticles showed similar degrees of accumulation within fibrin clots, emphasizing the importance of using targeting specificity controls in molecular imaging studies [29]. The pentapeptide CREKA has been shown to home micelles to the surface of atherosclerotic plaques, particularly to the shoulder regions of plaque where stability is compromised [10]. Incorporating Gd into CREKA-targeted peptide amphiphilic micelles allowed MR imaging of atherosclerotic plaques in $ApoE^{-/-}$ mice [30]. Although increasing signals were observed in vivo when CREKA-targeted peptide amphiphilic micelles were compared to non-targeted micelles, the quantitative results were not significantly different. This lack of significance could be due to many factors, including the dose administered, relative differences in micelle pharmacokinetics, the potential for protein-binding differences between micelles in vivo, and relative differences in phagocytic cell uptake in plaques. Safety should remain an important consideration for this approach. Initial studies utilizing CREKA-based iron oxide nanoparticles showed that clotting occurred in the lumen of tumor vasculature [31]. However, when CREKA peptides were presented in the form of micelles, clotting was not induced in vitro or in vivo [10]. Although this finding is promising, clotting is a key safety concern, especially in patients with atherosclerosis.

## Cellular Elements

As atherosclerotic plaques develop, cellular changes occur within them, including endothelial cell activation; smooth muscle cell proliferation and phenotypic changes; and recruitment, activation, and proliferation of leukocytes. Such cellular changes have recently been used as targets for nanoparticle imaging of atherosclerotic plaque.

### Endothelial Cells

VCAM-1 was one of the earliest targets identified for molecular imaging in patients with atherosclerosis because it was found to be upregulated on activated endothelial cells in plaque and to be responsible for leukocyte homing to plaques [14–16]. A wide variety of imaging modalities targeting VCAM-1 have been under development. These have ranged from high-affinity peptides and mAb for MR [32] or PET/CT imaging [33] to nanoparticles of iron oxide [34]. Most recently, Bruckman et al. [7] conjugated the VCAM-1-targeted peptide VHPKQHR [32] to tobacco mosaic virus (TMV) to take advantage of the non-spherical, rod-based supramolecular structure of the virus, which may facilitate vascular margination to endothelial surfaces and rapid clearance, both important characteristics of an imaging agent. When loaded with a near-infrared (NIR) dye and chelated Gd ions, the VCAM-1-targeted TMV enhanced $T_1$-weighted MR signals in the aorta of $ApoE^{-/-}$ mice more than non-targeted Gd-DOTA controls did (Fig. 4b), and immunofluorescence imaging showed selective staining of the cap of atherosclerotic plaques and little accumulation within subendothelial layers (Fig. 1c). Magnetic resonance imaging with non-targeted TMV controls was not performed in the $ApoE^{-/-}$ mice. Although the preclinical development of imaging agents targeting VCAM-1 has now

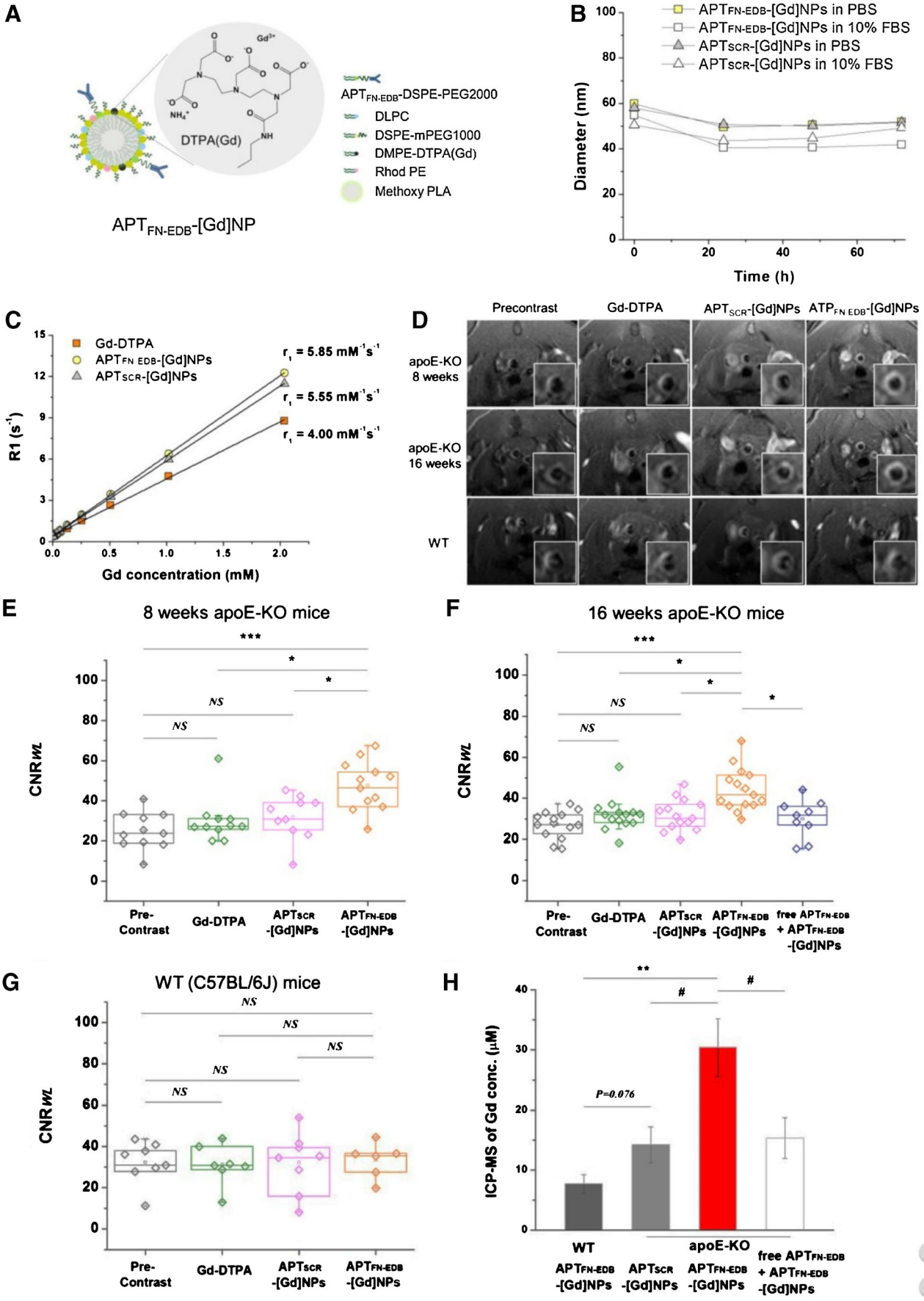
A
DTPA(Gd)
APTFN-EDB-DSPE-PEG2000
DLPC
DSPE-mPEG1000
DMPE-DTPA(Gd)
Rhod PE
Methoxy PLA
APTFN-EDB-[Gd]NP
B
APTFN-EDB-[Gd]NPs in PBS
APTFN-EDB-[Gd]NPs in 10% FBS
APTSCR-[Gd]NPs in PBS
APTSCR-[Gd]NPs in 10% FBS
Diameter (nm)
Time (h)
C
Gd-DTPA
APTFN EDB-[Gd]NPs
APTSCR-[Gd]NPs
r1 = 5.85 mM-1s-1
r1 = 5.55 mM-1s-1
r1 = 4.00 mM-1s-1
R1 (s-1)
Gd concentration (mM)
D
Precontrast
Gd-DTPA
APTSCR-[Gd]NPs
ATPFN EDB-[Gd]NPs
apoE-KO 8 weeks
apoE-KO 16 weeks
WT
E
8 weeks apoE-KO mice
CNRWL
Pre-Contrast
Gd-DTPA
APTSCR -[Gd]NPs
APTFN-EDB -[Gd]NPs
F
16 weeks apoE-KO mice
CNRWL
Pre-Contrast
Gd-DTPA
APTSCR -[Gd]NPs
APTFN-EDB -[Gd]NPs
free APTFN-EDB + APTFN-EDB -[Gd]NPs
G
WT (C57BL/6J) mice
CNRWL
Pre-Contrast
Gd-DTPA
APTSCR -[Gd]NPs
APTFN-EDB -[Gd]NPs
H
ICP-MS of Gd conc. (μM)
P=0.076
WT
apoE-KO
APTFN-EDB -[Gd]NPs
APTSCR -[Gd]NPs
APTFN-EDB -[Gd]NPs
free APTFN-EDB + APTFN-EDB -[Gd]NPs

◀ **Fig. 3** Atherosclerotic plaque detection ability of fibronectin-targeted nanoparticles ($APT_{FN-EDB}$-[Gd]NPs) is superior to that of Gd-DTPA or non-targeting NPs ($APT_{SCR}$-[Gd]NPs) in vivo. **a** Schematic of $APT_{FN-EDB}$-[Gd]NP. **b** In vitro stability of $APT_{FN-EDB}$-[Gd]NPs and $APT_{SCR}$-[Gd]NPs in phosphate-buffered saline (PBS) and 10% fetal bovine serum (FBS) at 37 °C. **c** The relaxivity (r1) of $APT_{FN-EDB}$-[Gd]NPs at 7.0 T. The r1 values for Gd-DTPA and $APT_{SCR}$-[Gd]NPs are also presented for comparison. **d**–**h** In vivo magnetic resonance imaging results of $APT_{FN-EDB}$-[Gd]NPs in ApoE-KO mice on a Western diet (WD) for 8 or 16 weeks or in wild-type (WT) mice (C57BL/6J) on a normal chow diet, compared with those of Gd-DTPA or $APT_{SCR}$-[Gd]NPs in the same animal models. **d** Representative cross-sectional views of brachiocephalic arteries obtained before and after injection of Gd-DTPA, $APT_{SCR}$-[Gd]NPs, or $APT_{FN-EDB}$-[Gd]NPs in each group. **e** Contrast normalized ratio (wall versus lumen) (CNR*WL*) values in ApoE-KO mice on an 8-week WD before (precontrast, $n = 11$) and after administration of Gd-DTPA ($n = 11$), $APT_{SCR}$-[Gd]NPs ($n = 10$), or $APT_{FN-EDB}$-[Gd]NPs ($n = 12$). **f** CNR*WL* values in ApoE-KO mice on a 16-week WD before (precontrast, $n = 14$) and after administration of Gd-DTPA ($n = 14$), $APT_{SCR}$-[Gd]NPs ($n = 14$), or $APT_{FN-EDB}$-[Gd]NPs ($n = 15$). Free $APT_{FN-EDB}$ was injected through the tail vein 2 h prior to the injection of $APT_{FN-EDB}$-[Gd]NPs ($n = 9$). **g** CNR*WL* values in WT mice before (precontrast, $n = 8$) and after administration of Gd-DTPA ($n = 7$), $APT_{SCR}$-[Gd]NPs ($n = 8$), or $APT_{FN-EDB}$-[Gd]NPs ($n = 6$). Data are for individual mice. The lower and upper ends of boxes represent the 25th and 75th percentiles, respectively, and the line across the box indicates the median. **h** Inductively coupled plasma mass spectrometry assessment of arteries collected from WT mice and ApoE-KO mice after administration of $APT_{FN-EDB}$-[Gd]NPs, $APT_{SCR}$-[Gd]NPs, or free $APT_{FN-EDB}$ + $APT_{FN-EDB}$-[Gd]NPs. $^{\#}P < 0.05$, $^{*}P < 0.005$, $^{**}P < 0.001$, $^{***}P < 0.0001$. NS, not significant. Adapted from Yu et al. [9] with permission

spanned over two decades, there is still no clinically accepted modality to non-invasively image VCAM-1 in patients.

Another possible approach to identify plaques susceptible to thrombosis is to use nanoparticles to image endothelial permeability. Stein-Merlob et al. [35] developed ultrasmall superparamagnetic iron oxide (USPIO) nanoparticles coated with cross-linked dextran conjugated to the NIR dye CyAM7 (CLIO-CyAM7). When CLIO-CyAM7 was administered to a balloon injury rabbit model of atherosclerosis, its accumulation in atheroma was diffusion-limited. When thrombosis was pharmacologically triggered in these animals (24 h after nanoparticle administration), CLIO-CyAM7 accumulation was found to be significantly greater in the thrombotic regions than in the non-thrombotic atheroma. Because intravascular NIR fluorescence imaging could be used to detect CLIO-CyAM7 in vessels with dimensions similar to those of human coronary arteries, it may be possible to use this minimally invasive approach to identify high-risk plaques in patients.

## Vascular Smooth Muscle Cells

There are limited descriptions of nanoparticle-based targeting of markers for vascular smooth muscle cells. Wang et al. [36] described a dual-modality fluorescence imaging method using iron oxide nanoparticles conjugated to polyclonal antibodies against profilin1 (PC-NPs), an actin-binding protein highly expressed in activated vascular smooth muscle cells in atherosclerotic plaques. Compared to control Ig-coated nanoparticles of similar design (IC-NPs), PC-NPs were selectively retained in plaques of $ApoE^{-/-}$ mice on a high-fat diet, as shown with both MR imaging and fluorescent staining. Although fluorescence imaging of plaques showed similar staining patterns with PC-NPs and IC-NPs, the overall fluorescence intensity was higher with PC-NPs, suggesting greater retention of these nanoparticles. Because profilin1 is an intracellular target, this finding suggests that this approach may be a method to image vascular smooth muscle cell necrosis, which has been described in atherosclerotic plaques [37].

## Immune Cells

The complexity and heterogeneity of the cellular microenvironment of an atherosclerotic plaque have been highlighted using new multidimensional technologies like mass cytometry, single-cell RNA sequencing, and laser capture microdissection [38–41]. A recent study using cytometry by time-of-flight (CyTOF) identified up to 23 different leukocyte subset clusters among single cells isolated from human carotid plaques after endarterectomy (Fig. 5a) [39]. This number of leukocyte clusters was comparable to the 22 clusters identified in the spleen using a similar methodology, highlighting the heterogeneity of the leukocyte population within plaques. The challenge is to identify cell subsets that correlate with plaque instability and develop a means to identify these cell types in patients for risk stratification. Along these lines, Winkels et al. [39] identified a cluster of $CD4^{+}$ T cells that, based on transcriptional profiling, were related to memory T cells. The prevalence of these cells inversely correlated with ischemic events after thromboendarterectomy, suggesting they have a protective role, whereas macrophage prevalence showed a weak positive correlation to ischemic events. Although the techniques used by Winkels et al. allowed for a higher resolution analysis of immune cell clusters in atheromas, the relative abundance of each major leukocyte lineage found in the human lesions remained similar to the levels previously reported by others [17]. Macrophages and monocytes make up the majority of the population, followed by T cells, B cells, and NK cells.

### Macrophages/Monocytes

Monocytes are recruited into nascent LDL-enriched inflammatory sites in coronary and carotid arteries. Once

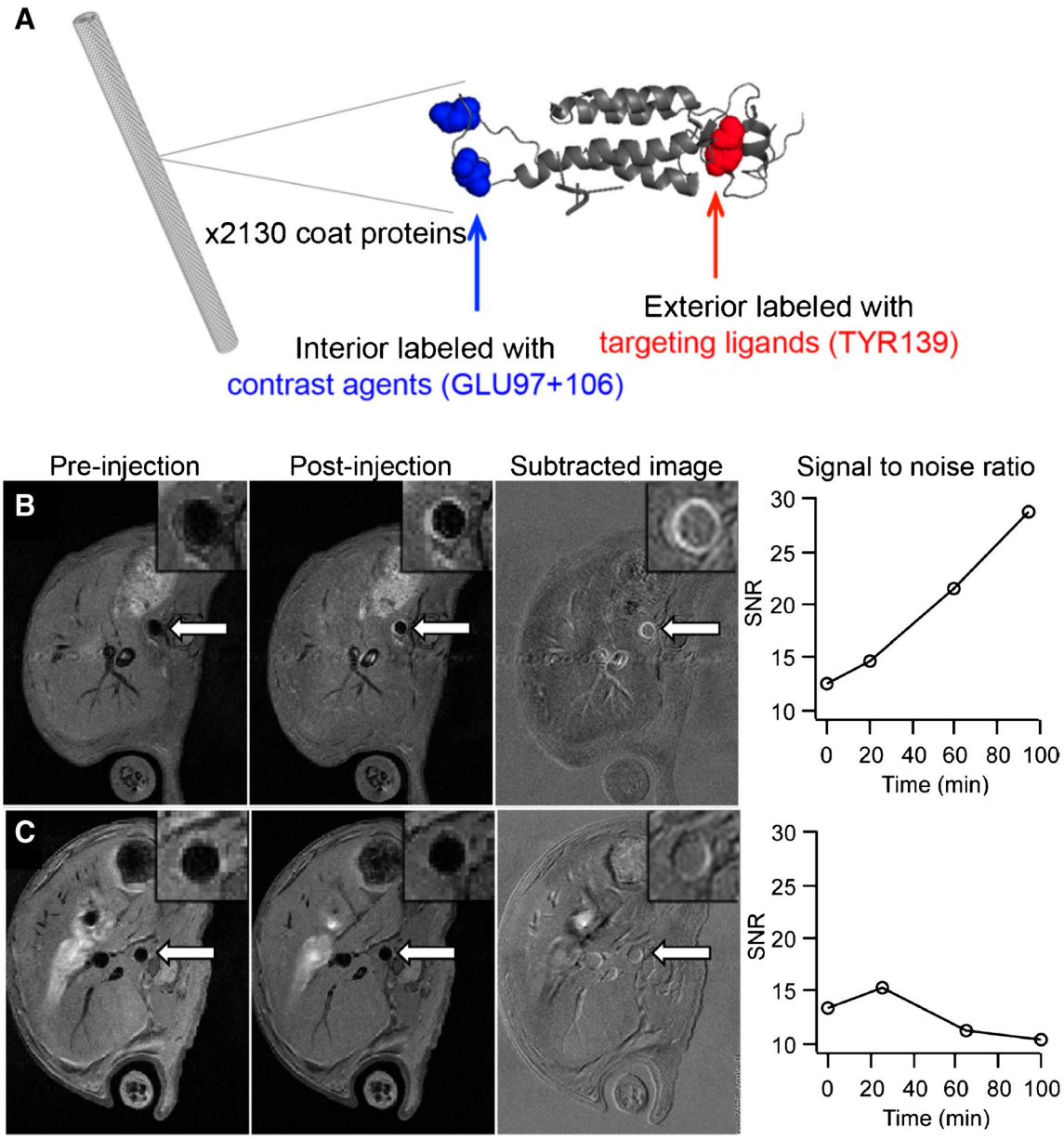


**Fig. 4** **a** An illustrative image (PyMol and Chimera) of the structure of tobacco mosaic virus (TMV) rods and the coat protein. The exterior (red) and interior (blue) reactive amino acids are highlighted in the individual coat protein. **b**, **c** Pre- and post-injection magnetic resonance imaging scans of VCAM-1-targeted TMV in an ApoE$^{-/-}$ mouse (**b**) and a C57Bl/6 mouse (**c**). The third column is the subtracted image (90 min post-injection minus pre-injection). The fourth column is the signal-to-noise ratio (SNR) for the vessel wall of the aortas. Insets are magnified images of the abdominal aorta regions of interest. Adapted with permission from Bruckman et al. [7]

there, they become activated and differentiate into macrophages and foam cells, ramping up inflammation that can ultimately lead to plaque destabilization. Most nanoparticle-based imaging probes (ex, iron oxides, liposomes, micelles, and lipoproteins) target macrophages. This is either by design, through molecular targeting, or by default, as a result of the high phagocytic activity of this cell type.

Recent studies aimed at imaging monocytes/macrophages in animal models of atherosclerosis have analyzed modified dextran nanoparticles, polyglucose nanoparticles, HDL nanoparticles, and dendrimers [42]. Majmudar et al. [43] have described the use of dextran nanoparticles functionalized through covalent modifications with a $^{89}$Zr chelator and fluorophore (VivoTag680) to image plaque inflammation by PET/MR in an ApoE$^{-/-}$ model of atherosclerosis (Fig. 6). Notably, almost 90% of the cellular uptake of the nanoparticles in the plaques was in the monocyte/macrophage and neutrophil cell lineages (Fig. 6k). A significant decrease in PET signal was noted

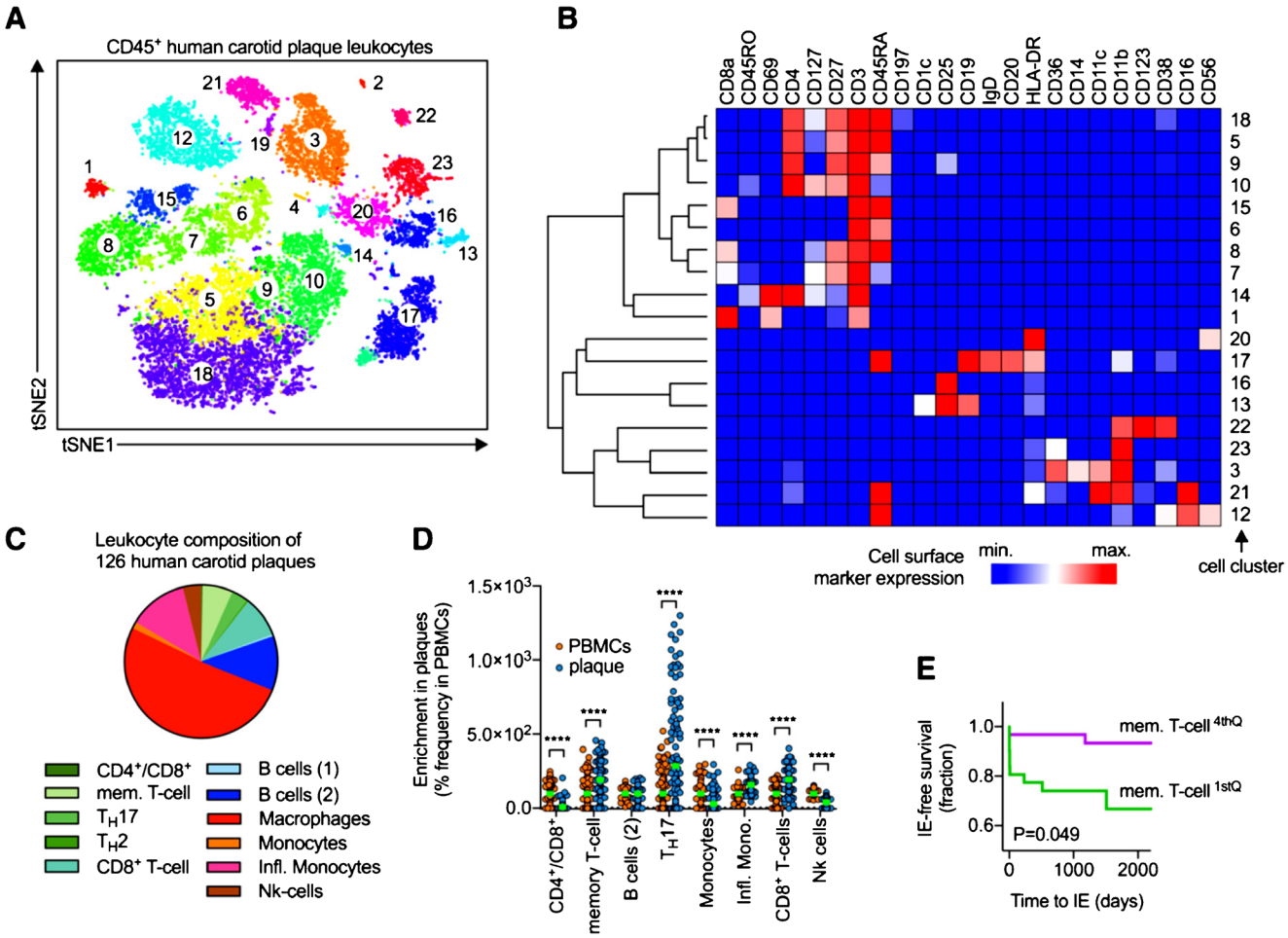


**Fig. 5** The frequency of aortic leukocyte populations predicts clinical events in patients with atherosclerosis. **a** Unsupervised cell cluster detection by a modified t-distributed stochastic neighbor embedding (tSNE) and cytometry by time-of-flight (CyTOF) cluster detection algorithm (PhenoGraph) on $CD45^+$, live, $DNA^+$ leukocytes from human carotid plaques after endarterectomy and staining with an anti-human antibody panel and acquisition in CyTOF. **b** Median expression of surface markers per cluster shown in a hierarchically clustered heatmap (row and column). A cluster frequency of > 1% $CD45^+$, live, $DNA^+$ events was applied. The heatmap was normalized across clusters. **c** Genetic deconvolution of leukocyte cluster gene signatures in a set of bulk mRNA expression arrays of 126 human carotid plaques from the Biobank of Karolinska Endarterectomies to enumerate the relative abundance of cell clusters. The relative frequency of the tested clusters is shown. **d** Relative enrichment of leukocyte populations in plaques vs peripheral blood mononuclear cells (PBMCs) displayed as percentage of the frequency within PBMCs. $n > 97$ per group. Data are presented as mean ± SEM. **e** Kaplan-Meier survival curves of ischemic event (IE)-free survival after thromboendarterectomy. Myocardial infarction and stroke were classified as ischemic events. The patients were separated into quartiles according to the memory T cell frequency in their plaque samples, and those in the lowest quartile (1stQ) and highest quartile (4thQ) were compared. Number of IEs: 1stQ = 9 and 4thQ = 2. Significance was determined by a two-sided, unpaired Student's *t* test (**d**). $^{****}P < 0.0001$ (**d**) or in both a log-rank and Gehan-Breslow-Wilcoxon test for survival curves (**e**). Infl., inflammatory; mem., memory; Nk cells, natural killer cells. Adapted with permission from Winkels et al. [39]

upon siRNA-mediated silencing of CCR2, a G protein-coupled receptor associated with monocyte recruitment to plaques [43]. The blood half-life of $^{89}$ZR-conjugated dextran nanoparticles was approximately 4 h [43]. Nanoparticles have been developed that are smaller than the renal excretion threshold, decreasing their circulating half-lives, which has allowed them to be used with radio-isotopes that have faster decay times, like the clinically translatable radioisotope $^{18}$F. Keliher et al. [44] designed modified polyglucose-based nanoparticles that averaged 5 nm in diameter. Biodistribution studies confirmed primary renal elimination of these nanoparticles, resulting in rapid elimination and a blood half-life of 6.5, 22.5, and 21.7 min in mice, rabbits, and primates, respectively. Use of the $^{18}$F-modified polyglucose nanoparticles ($^{18}$F-Macroflor) enabled PET/CT imaging of macrophages in the plaques of atherosclerotic $ApoE^{-/-}$ mice (Fig. 7a) and rabbits. Interestingly, uptake of this nanoparticle by plaque macrophages demonstrated a bimodal distribution, with approximately half of the macrophage population

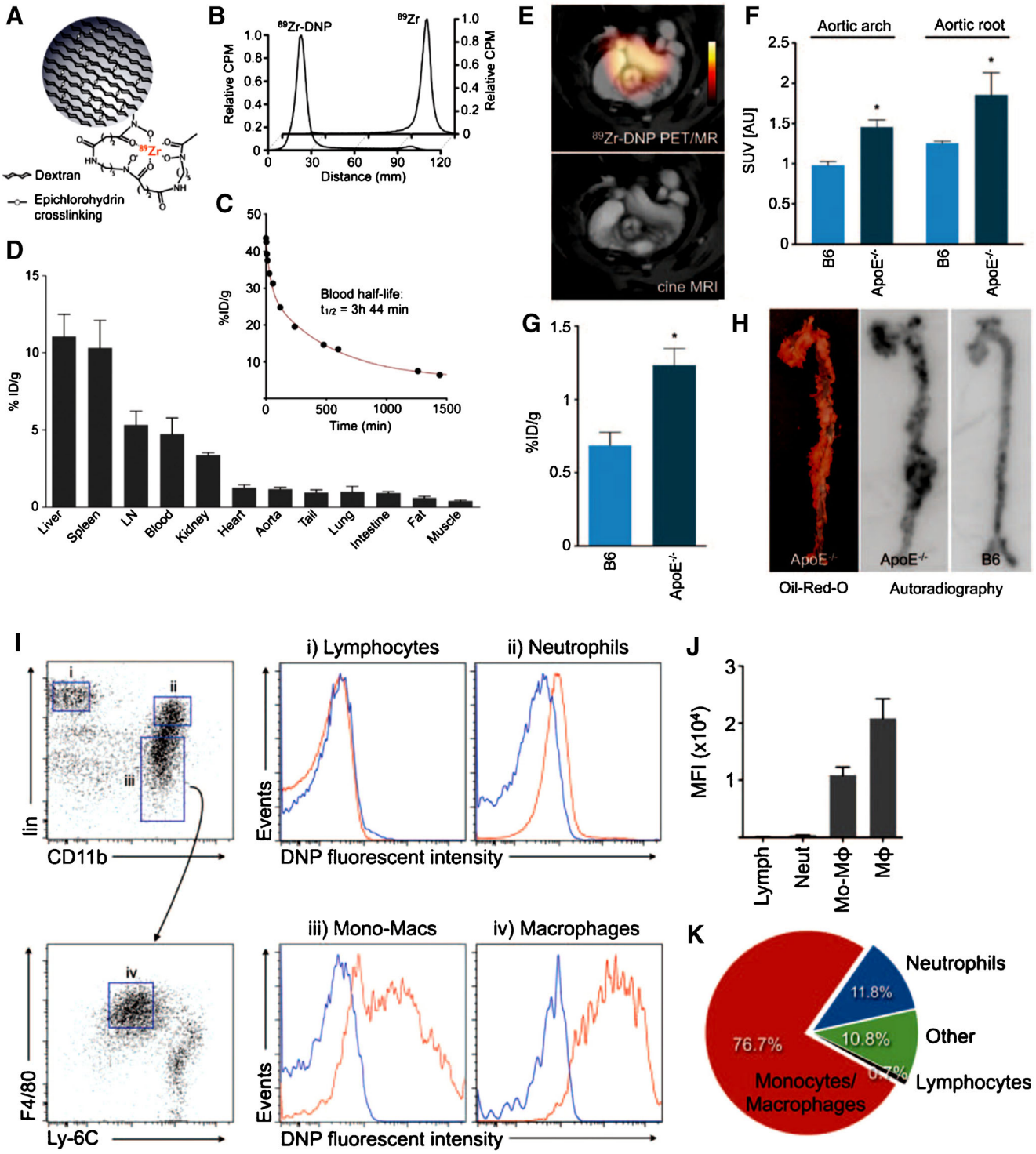


showing high nanoparticle incorporation and half showing little to no nanoparticle incorporation (Fig. 7h). No uptake occurred in the neutrophils. In contrast, functionalized dextran nanoparticles described by Majmudar et al. [43] appeared to be present in all the macrophages and neutrophils from aortic plaques. Perhaps, future studies using multidimensional technologies like mass cytometry will be able to identify with greater definition the exact nature of the cellular subsets (leukocytes and others) labeled by nanoparticles such as these.

Another approach to imaging monocytes/macrophages has been modeled after a naturally occurring nanoparticle, HDL.

◀ **Fig. 6** **a** Schematic representation of a dextran-coated nanoparticle with a $^{89}$Zr chelator. **b** Radio thin-layer chromatography traces for zirconium-89-radiolabeled dextran nanoparticles ($^{89}$Zr-DNP) and $^{89}$Zr. **c** Blood half-life of $^{89}$Zr-DNP. **d** Biodistribution of $^{89}$Zr-DNP 48 h after intravenous administration ($n = 5$). **e** Representative hybrid positron emission tomography (PET)/magnetic resonance (MR) image of an ApoE$^{-/-}$ mouse aortic valve (top). Cine MR imaging frame of aortic valve (bottom). **f** In vivo PET signal in the aortic arch and root in wild-type C57BL/B6 mice (B6) and ApoE$^{-/-}$ mice with atherosclerosis ($n = 4$–5 per group). **g** Scintillation counting of excised aortas corroborated data from in vivo PET/MR imaging. Data are normalized for weight, radioactive decay, and injected dose. For **f** and **g**, data are presented as mean ± SEM, $^{*}P < 0.05$. **h** Oil-Red-O staining (left) and autoradiography (middle and right) of excised aortas. **i** The plot on the far left shows gates for (i) lymphocytes, (ii) neutrophils, (iii) mononuclear phagocytes, and (iv) macrophages from single-cell aortic suspensions. The histograms show the respective intracellular signal in the VT680 FACS channel, which represents DNP uptake by the cells. Blue histograms indicate the signal in uninjected control ApoE$^{-/-}$ mice, whereas red histograms indicate signal from cells retrieved from ApoE$^{-/-}$ mice after DNP injection ($n =$ 3 per group). **j** Bar graph of mean fluorescence intensity (MFI) in different leukocytes. **k** Pie chart showing the relative signal contribution per cell type. CPM, counts per minute; DNP, dextran nanoparticles; %ID/g, percent injected dose per gram tissue; LN, lymph nodes; lymph, lymphocytes; Mo, monocytes; Mϕ, macrophages; neut, neutrophils; SUV, standard uptake values. Adapted with permission from Majmudar et al. [43]

Perez-Medina et al. [21] generated HDL mimetics containing the primary constituents of HDL, 1,2-dimyristoyl-sn-glycero-3-phosphocholine (DMPC), and ApoA-I, and modified them with the PET imaging agent $^{89}$Zr or the NIR fluorophore Cy5.5. In murine, rabbit, and porcine models of atherosclerosis, use of these HDL mimetics significantly enhanced the PET signal in the lesions, and this enhancement correlated with uptake of these nanoparticles by monocytes, macrophages, and neutrophils [21]. HDL mimetics have rapidly progressed into clinical trials for use as bioactive nanotherapeutics because they have been shown to have atheroprotective properties in animal models; these properties have been ascribed, in part, to their ability to promote reverse cholesterol efflux from plaque macrophages [45, 46]. Unfortunately, in the clinical trials to date, HDL mimetics have not been shown to reverse atherosclerotic plaques in patients [47, 48]. However, in one clinical study that utilized the $^{89}$Zr-labeled HDL mimetic CDR-001, the PET signal was enhanced in atherosclerotic plaques, suggesting that HDL mimetic nanoparticles may have utility in imaging inflammatory burden in patients [49] and may be able to serve as drug delivery vehicles [50, 51]. HDL mimetic nanoparticles remain one of the few nanoparticle imaging agents used in humans that are not iron oxide-based.

Targeting and uptake of nanoparticles by macrophages/monocytes typically rely on scavenger receptors and pattern recognition receptors, nanoparticle "protein corona" opsonization, or, in the case of HDL mimetic nanoparticles, ATP-binding cassette transporters. Molecular-targeted delivery of nanoparticles has been described recently. USPIO nanoparticles targeted to lectin-like oxidized LDL receptor 1 (LOX-1) with an anti-LOX-1 mAb demonstrated significant hypointense MR signals in carotid plaques of ApoE$^{-/-}$ mice when compared to non-targeted, IgG-conjugated control USPIO [52]. Although LOX-1 is expressed by macrophages in plaques, it can also be expressed by vascular smooth muscle cells and fibroblasts [53]. Other molecular targets that can detect monocytes/macrophages include CD36 [54], CD163 [55], hyaluronan receptors [56], pan pro-inflammatory chemokine receptors [57], phosphatidylserine and other "eat-me" signals (reviewed by Bagalkot et al. [58]), and folate receptors [59]. Although many of these targeted nanoparticles have shown enhanced accumulation in atherosclerotic plaques compared to control nanoparticles, it is not clear whether these various targeting approaches can differentiate between specific macrophage subsets or whether the specific macrophage subsets detected are indicative of unstable plaques.

One approach our laboratory has taken to image the inflammatory burden of plaques is to target the receptor on leukocytes that is responsible for homing these cells to plaques [6]. This receptor is the integrin cell adhesion molecule α4β1 (also called very late activation antigen-4 [VLA-4]), which binds the counter ligand VCAM-1. As stated above, the α4β1/VCAM-1 adhesion axis is responsible for homing leukocytes to plaques [14–16]. By modifying a selective, high-affinity, small-molecule antagonist of the integrin α4β1 with a PEGylated phospholipid, we have generated a liposome-based nanoparticle (THI567-targeted liposome-Gd) that becomes incorporated into circulating monocytes, T cells, B cells, and, to a lesser extent, neutrophils, within hours of intravenous administration (Fig. 8c–f) [6], which differentiates it from others that are poorly taken up by lymphocytes. In ApoE$^{-/-}$ mice on a high-fat diet, contrast within the aortic wall was significantly enhanced when MR imaging was performed with α4β1-targeted Gd-loaded liposomes rather than non-targeted liposomes. The MR imaging was performed on a 1-T scanner, suggesting that clinical translation of this technique is feasible (Fig. 9). This imaging approach has the potential to show the total inflammatory burden of plaques, and it would be of interest to explore this modality further to analyze vascular inflammation in plaques under different therapeutic conditions. Also, since integrins readily internalize through clathrin-dependent and clathrin-independent pathways [60], this is a novel approach to drug delivery that could affect not only monocytes/macrophages and neutrophils but also T cells and B cells.

## T and B Cells

Given that lymphocytes make up a significant percentage of the immune cells in an atherosclerotic plaque, it is important to

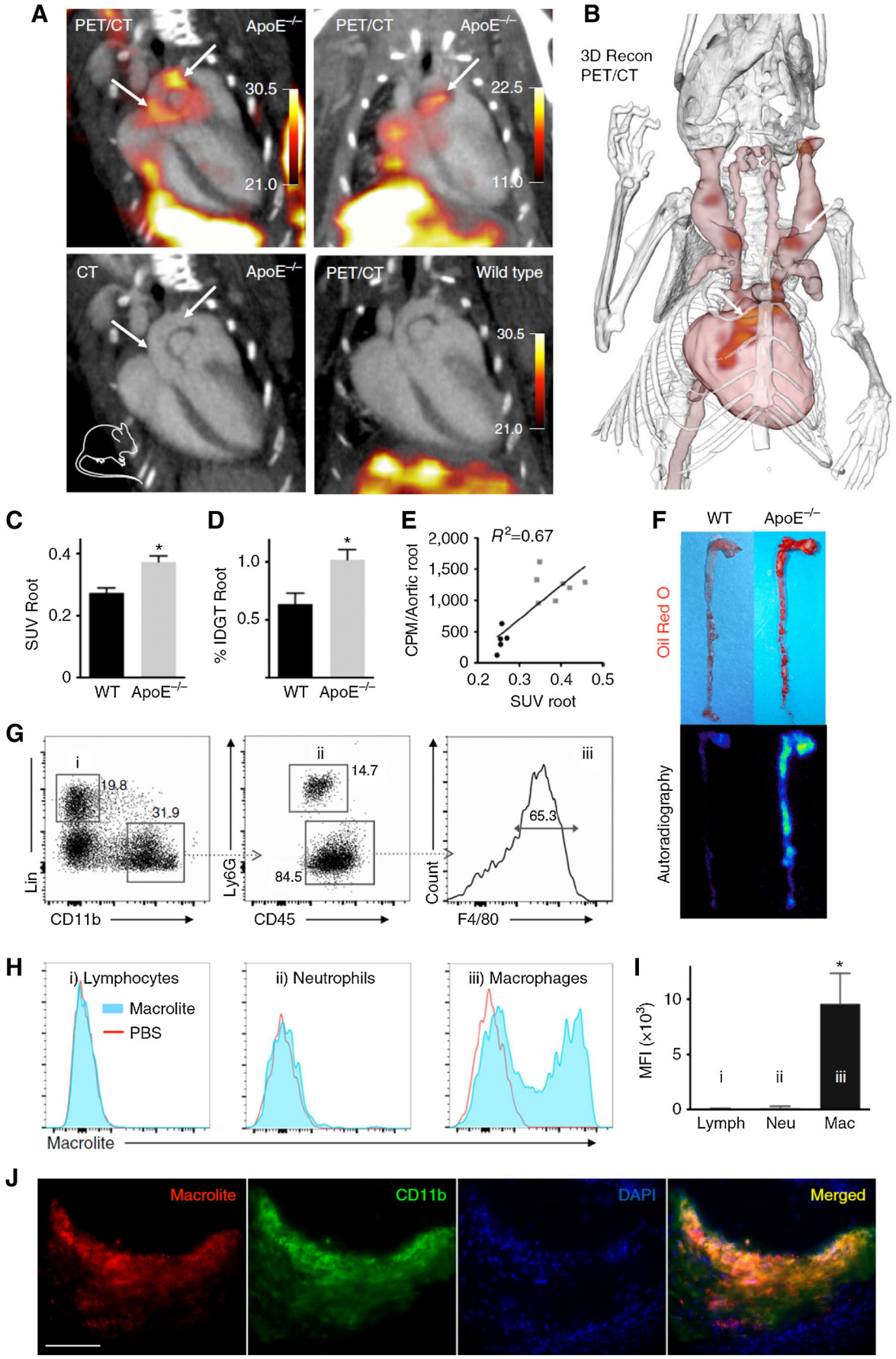
A
PET/CT
ApoE−/−
30.5
21.0
PET/CT
ApoE−/−
22.5
11.0
CT
ApoE−/−
PET/CT
Wild type
30.5
21.0
B
3D Recon
PET/CT
C
SUV Root
0.4
0.2
0
WT
ApoE−/−
D
% IDGT Root
1.0
0.5
WT
ApoE−/−
E
R2=0.67
CPM/Aortic root
2,000
1,500
1,000
500
0
0.2
0.3
0.4
0.5
SUV root
F
WT
ApoE−/−
Oil Red O
Autoradiography
G
i
19.8
31.9
Lin
CD11b
ii
14.7
84.5
Ly6G
CD45
iii
65.3
Count
F4/80
H
i) Lymphocytes
Macrolite
PBS
ii) Neutrophils
iii) Macrophages
Macrolite
I
MFI (×10³)
10
5
0
i
ii
iii
Lymph
Neu
Mac
J
Macrolite
CD11b
DAPI
Merged

◀ **Fig. 7** Positron emission tomography (PET)/computed tomography (CT) with $^{18}$F-Macroflor, a modified polyglucose nanoparticle, to image macrophages in aortic plaques of mice with atherosclerosis. **a** Representative PET/CT images of several experiments in ApoE$^{-/-}$ and wild-type control mice after intravenous (IV) injection of $^{18}$F-Macroflor ($n = 14$). PET scale bar is in kBq/cc. **b** Three-dimensional rendering derived from PET/CT in ApoE$^{-/-}$ mouse shows PET signal in red (arrows). **c** In vivo standard uptake values (SUV) for aortic roots of wild-type and ApoE$^{-/-}$ mice ($n = 5$–7 per group, unpaired $t$ test). **d** Ex vivo gamma count reports percent injected dose per gram aortic tissue (%IDGT) ($n = 5$–7 per group, unpaired $t$ test). **e** Correlation between **c** and **d** for individual wild-type (black) and ApoE$^{-/-}$ mice (gray). CPM, counts per minute. **f** Ex vivo Oil-Red-O staining and corresponding autoradiography of representative aortas. **g** Flow cytometric gating of aortic cells after IV injection of Macrolite (a fluorescent, non-radioactive version of $^{18}$F-Macroflor). **h** Mean fluorescence intensity (MFI) of Macrolite in lymphocytes, neutrophils, and macrophages retrieved from ApoE$^{-/-}$ mouse aorta. **i** VT680 fluorescence indicating Macrolite uptake. Cells obtained from three ApoE$^{-/-}$ mouse aortas (one-way analysis of variance). **j** Fluorescence microscopy of aortic root plaque after IV injection of Macrolite. Scale bar = 100 mm. In **c**, **d**, and **i**, data are shown as mean ± SEM, $^{*}P < 0.05$. Mouse cartoon image is reproduced from the Servier Medical Art image databank (http://www.servier.com/Powerpoint-image-bank). Adapted from Keliher et al. [44] with permission

develop tools to monitor these cell types in patients with this inflammatory disease. Despite this, the recent literature includes very few descriptions of nanoparticle-based imaging probes that specifically target T cells or B cells. In a collagen-induced arthritis model in rats, Chen et al. [61] used iron oxide nanoparticles functionalized with an anti-CD3 mAb for MR imaging and found that his agent caused significant hypointense signals in inflamed joints. The regions of MR signal change and CD3-targeted nanoparticle localization correlated with the sites of T cell accumulation in the inflammatory joints, as determined with immunohistochemistry. Imaging of B cell malignancies in vivo has been accomplished with poly-lactic acid-based nanoparticles conjugated to anti-CD20 antibodies [62]. In this study, human MEC1 B cell tumors were first established subcutaneously in SCID mice. The mice that subsequently received intravenous injections of CD20-targeted nanoparticles had significantly greater fluorescent signals within the tumors than the mice that received non-targeted control nanoparticles, suggesting that specificity was due to the CD20 targeting. Neither of the nanoparticles described above has been tested in animal models of atherosclerosis. Techniques for imaging lymphocytes in inflammatory plaques are still needed.

### Neutrophils

Although neutrophils have been known to be components of culprit lesions [63], only recently has the role of neutrophils in plaque destabilization been emphasized [64]. This has coincided with the observation that neutrophil extracellular traps (NETs) are present in all types of unstable plaque, including ruptures, erosions, and intraplaque hemorrhage [65]. Neutrophil extracellular traps are the result of neutrophil activation and degranulation of a matrix comprising chromatin and granule components [66]. In atherosclerotic plaques, NETs are usually found on the luminal surface of culprit lesions [64], suggesting that imaging NET components may be as simple as imaging endothelial markers like VCAM-1. However, at present, there are no nanoparticle-based agents specifically developed to target neutrophil NETs. In fact, there are very few technologies available to specifically target neutrophils themselves. One approach has been to incorporate as a targeting component the *N*-cinnamoyl-F-(D)L-F-(D)L-F (cFLFLF) peptide, a high-affinity antagonist of formyl peptide receptor 1 (FPR-1), which is expressed on neutrophils. In one study, $^{68}$Ga-labeled nanoparticles were conjugated to cFLFLFL and tested in an LPS-dependent murine model of lung inflammation [67]. In these animals, radiotracer was readily observed in the lungs with PET imaging. LPS-treated animals that were neutrophil depleted with Ly6G antibody showed a lack of signal in the lungs, suggesting that the positive signals were specific for neutrophils and not due to other myeloid-derived inflammatory cells that can express FPR-1. Testing of this neutrophil-specific nanoparticle in atherosclerotic models has not been reported.

## Conclusion

The number of small-molecule and nanoparticle-based agents and modalities available for imaging inflammation at the preclinical level is staggering [2, 3]. Yet, a clinically proven, non-invasive means to identify plaques that are unstable and prone to thrombosis is still not available. This is due, in part, to the relatively high safety hurdle for diagnostic agents compared to that for therapeutic agents, as the former have the potential to harm otherwise healthy individuals. Perhaps, this is why most imaging agents used in patients with CVD have originated from clinical developments in oncology.

Nanoparticle technologies offer significant advantages over small-molecule chelator or radiotracer approaches in clinical settings. These include lack of radiation exposure, concentrated imaging agent delivery, enhanced MR signal contrast by limiting diffusion of molecules like Gd, limited contrast agent toxicities, and the potential for therapeutic payload delivery. It is this latter characteristic that has rapidly driven mimetics of a naturally occurring nanoparticle, HDL, into clinical testing.

Designing nanomaterials that can specifically target inflammatory cells other than monocytes and macrophage would help improve our understanding of the pathogenesis of disease in animal models and help guide the development of novel treatment strategies for patients because lymphocytes and neutrophils are present in significant numbers in human plaques.

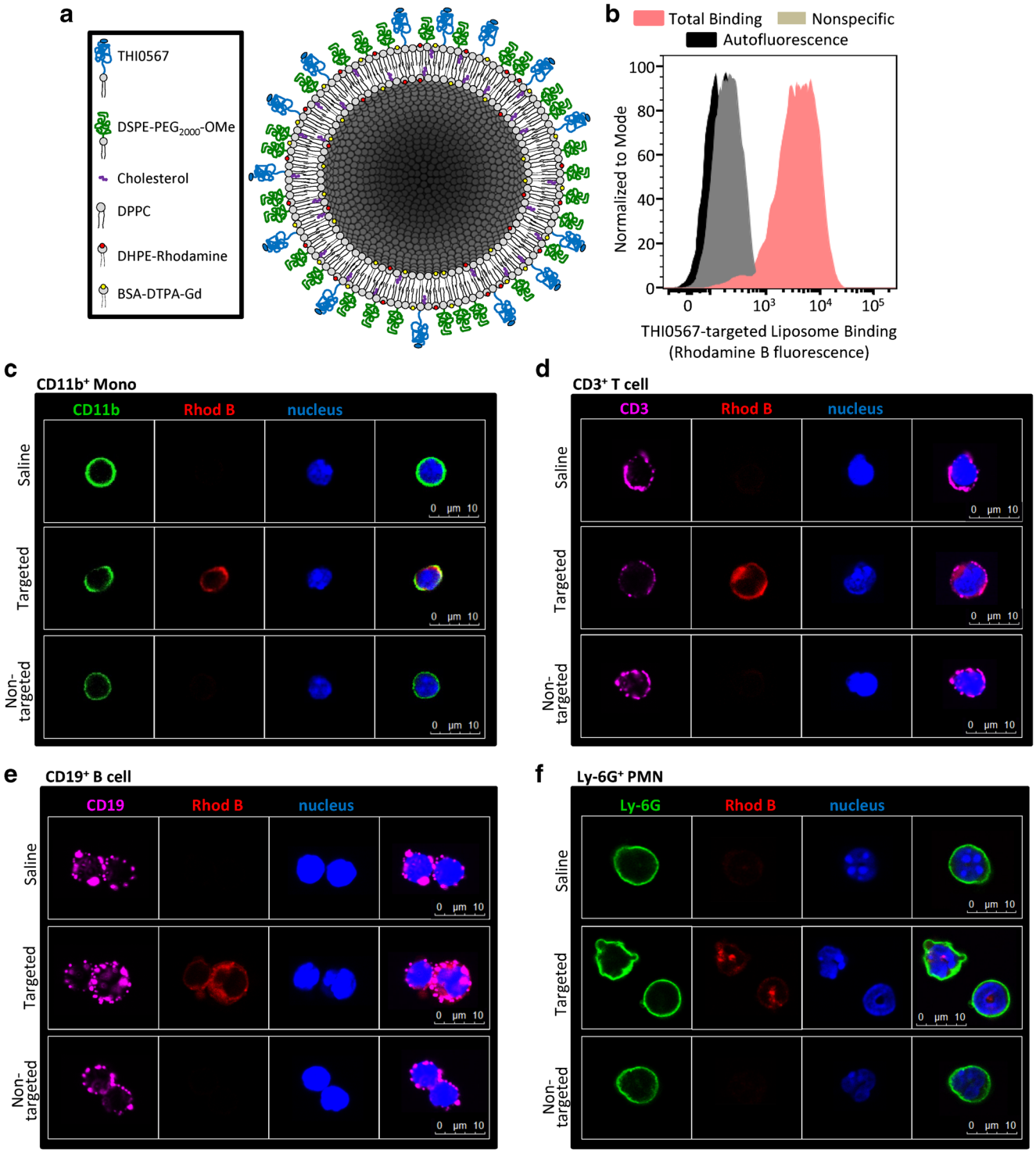


**Fig. 8** Integrin α4β1-targeted liposomes. **a** Schematic diagram of liposome formulation. **b** Flow cytometric analysis of THI0567-targeted liposome-Gd binding to Jurkat cells. **c**–**f** Confocal imaging of liposome binding to sorted peripheral blood cells after intravenous administration of the liposomes. After cytometry and sorting, confocal microscopy was performed to show CD11b (FITC) (**c**), CD3 (Cy5) (**d**), CD19 (Cy5) (**e**), Ly-6G (FITC) (**f**), Rhodamine B (to identify liposomes), and Hoechst 33342 (nucleus stain). Identical confocal acquisition settings were used for all images. For all experiments, targeted liposome = THI0567-targeted liposomal-Gd; non-targeted = liposomal-Gd. CD, cluster of differentiation; DPPC, dipalmitoyl phosphatidylcholine; DHPE-Rhodamine, dihexadecanoyl phosphoethanolamine (Lissamine rhodamine B); DSPE-PEG2000-OMe, distearoyl phosphoethanolamine-methoxy-polyethylene glycol2000; DTPA-BSA-Gd, diethylene triamine pentaacetic acid-bis(stearylamide) (gadolinium); PMN, polymorphonuclear; THI0567, distearoyl phosphoethanolamine-methoxy-polyethylene glycol3400-linker-THI0565. Adapted from Woodside et al. [6] with permission

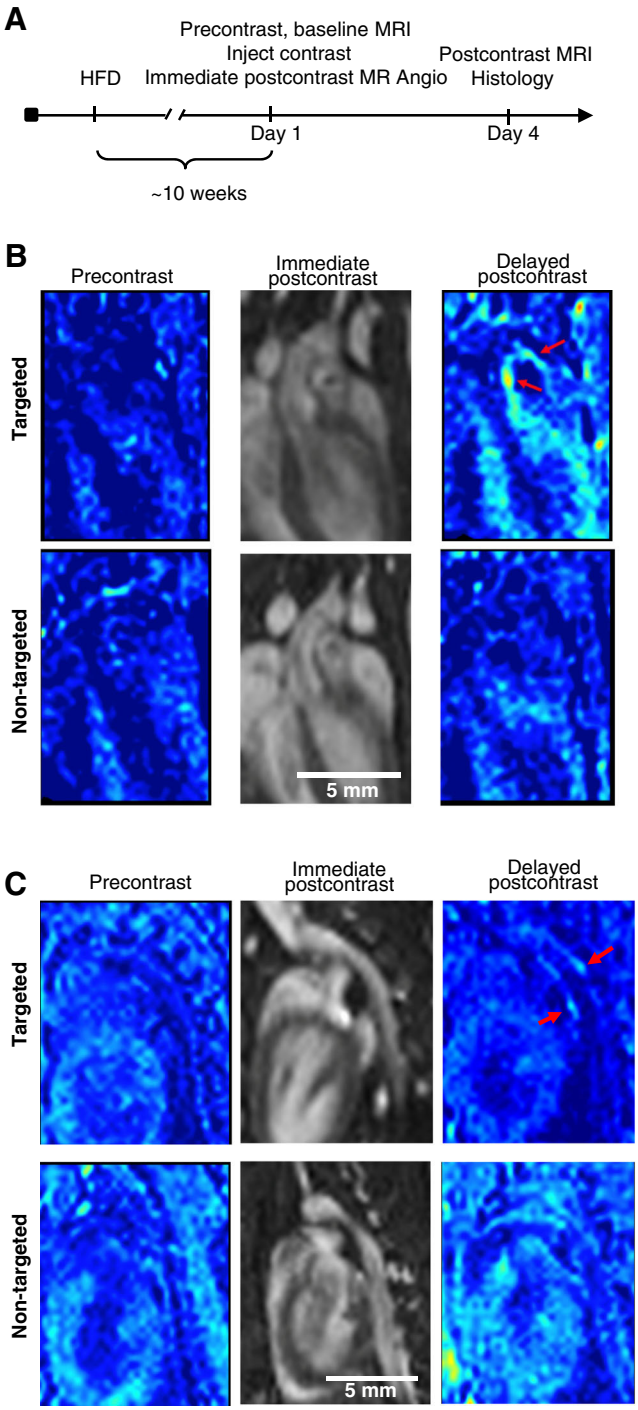


◀ **Fig. 9** In vivo magnetic resonance (MR) imaging of THI0567-targeted liposomal-Gd in atherosclerotic plaques. **a** Timeline for MR imaging studies. ApoE$^{-/-}$ mice (12–14 weeks old) were fed a high-fat diet (HFD) for ~10 weeks before imaging was initiated. Magnetic resonance imaging was performed at three time points: (1) precontrast, (2) immediate post-contrast (within 1 h of contrast administration to acquire an angiogram of the aorta), and (3) delayed post-contrast (at 72 h after contrast administration). **b** Representative coronal T1-weighted pseudo-colored MR images of the aortic arch from a THI0567-targeted liposomal-Gd-treated mouse (top row) and a non-targeted liposomal-Gd-treated mouse (bottom row) at baseline, immediate post-contrast, and delayed post-contrast. Signal enhancement within the aortic arch wall in a THI0567-targeted liposomal-Gd-treated mouse (red arrow) is shown. **c** Representative coronal T1-weighted pseudo-colored MR images of the descending aorta from a THI0567-targeted liposomal-Gd-treated mouse (top row) and a non-targeted liposomal-Gd-treated mouse (bottom row). Signal enhancement is seen in the aortic wall in the THI0567-targeted liposomal-Gd-treated mouse (red arrows). Adapted from Woodside et al. [6] with permission

Superficial plaque erosions are structurally different from plaques that have undergone rupture; they have less macrophage/foam cell content, more vascular smooth muscle cells, and more ECM [18], and they are more common in patients taking statins. Testing of nanoparticle-based imaging agents in animal models should include assessments of this different plaque phenotype.

Nanoparticle-based techniques for imaging inflammation in atherosclerotic plaque are ready to transition from preclinical testing in animal models to clinical use. By combining different targeted platforms with multimodality imaging, the ability to accurately risk stratify patients and guide clinical development of novel treatment strategies is within reach.

**Acknowledgments** The author would like to thank Peter Vanderslice, PhD, for critical review of the manuscript, and Heather Leibrecht, MS, ELS, of The Texas Heart Institute for editorial assistance in the preparation of the manuscript.

## Compliance with Ethical Standards

**Conflict of Interest** Dr. Woodside has a patent pending, PCT/US18/29991—Targeting Nanoparticles, and he is a co-founder of and investor in 7Hills Pharma, LLC, a startup biotechnology company developing novel immunotherapies for cancer.

**Human and Animal Rights and Informed Consent** The article reviews work previously published by the author that involved animals. There are no unpublished animal studies included in this article.

## References

1. World Health Organization. The top 10 causes of death. http://www.who.int/news-room/fact-sheets/detail/the-top-10-causes-of-death. Acessed 15 Jan 2019.
2. Vigne J, Thackeray J, Essers J, Makowski M, Varasteh Z, Curaj A, et al. Current and emerging preclinical approaches for imaging-based characterization of atherosclerosis. Mol Imaging Biol. 2018;20(6):869–87. https://doi.org/10.1007/s11307-018-1264-1.
3. Smith BR, Gambhir SS. Nanomaterials for in vivo imaging. Chem Rev. 2017;117(3):901–86. https://doi.org/10.1021/acs.chemrev.6b00073.
4. Ridker PM, Everett BM, Thuren T, MacFadyen JG, Chang WH, Ballantyne C, et al. Antiinflammatory therapy with canakinumab for atherosclerotic disease. N Engl J Med. 2017;377(12):1119–31. https://doi.org/10.1056/NEJMoa1707914.
5. Koenig W. Inflammation revisited: atherosclerosis in the post-CANTOS era. Eur Cardiol. 2017;12(2):89–91. https://doi.org/10.15420/ecr.2017:18:1.

6. Woodside DG, Tanifum EA, Ghaghada KB, Biediger RJ, Caivano AR, Starosolski ZA, et al. Magnetic resonance imaging of atherosclerotic plaque at clinically relevant field strengths (1T) by targeting the integrin alpha4beta1. Sci Rep. 2018;8(1):3733. https://doi.org/10.1038/s41598-018-21893-x.
7. Bruckman MA, Jiang K, Simpson EJ, Randolph LN, Luyt LG, Yu X, et al. Dual-modal magnetic resonance and fluorescence imaging of atherosclerotic plaques in vivo using VCAM-1 targeted tobacco mosaic virus. Nano Lett. 2014;14(3):1551–8. https://doi.org/10.1021/nl404816m.
8. Chen W, Cormode DP, Vengrenyuk Y, Herranz B, Feig JE, Klink A, et al. Collagen-specific peptide conjugated HDL nanoparticles as MRI contrast agent to evaluate compositional changes in atherosclerotic plaque regression. JACC Cardiovasc Imaging. 2013;6(3):373–84. https://doi.org/10.1016/j.jcmg.2012.06.016.
9. Yu M, Ortega CA, Si K, Molinaro R, Schoen FJ, Leitao RFC, et al. Nanoparticles targeting extra domain B of fibronectin-specific to the atherosclerotic lesion types III, IV, and V-enhance plaque detection and cargo delivery. Theranostics. 2018;8(21):6008–24. https://doi.org/10.7150/thno.24365.
10. Peters D, Kastantin M, Kotamraju VR, Karmali PP, Gujraty K, Tirrell M, et al. Targeting atherosclerosis by using modular, multifunctional micelles. Proc Natl Acad Sci U S A. 2009;106(24):9815–9. https://doi.org/10.1073/pnas.0903369106.
11. Tall AR, Yvan-Charvet L. Cholesterol, inflammation and innate immunity. Nat Rev Immunol. 2015;15(2):104–16. https://doi.org/10.1038/nri3793.
12. Nakayama M. Macrophage recognition of crystals and nanoparticles. Front Immunol. 2018;9:103. https://doi.org/10.3389/fimmu.2018.00103.
13. Hansson GK, Libby P, Tabas I. Inflammation and plaque vulnerability. J Intern Med. 2015;278(5):483–93. https://doi.org/10.1111/joim.12406.
14. Cybulsky MI, Gimbrone MA Jr. Endothelial expression of a mononuclear leukocyte adhesion molecule during atherogenesis. Science. 1991;251(4995):788–91.
15. Cybulsky MI, Iiyama K, Li H, Zhu S, Chen M, Iiyama M, et al. A major role for VCAM-1, but not ICAM-1, in early atherosclerosis. J Clin Invest. 2001;107(10):1255–62. https://doi.org/10.1172/JCI11871.
16. Patel SS, Thiagarajan R, Willerson JT, Yeh ET. Inhibition of alpha4 integrin and ICAM-1 markedly attenuate macrophage homing to atherosclerotic plaques in ApoE-deficient mice. Circulation. 1998;97(1):75–81.
17. Galkina E, Ley K. Immune and inflammatory mechanisms of atherosclerosis (*). Annu Rev Immunol. 2009;27:165–97. https://doi.org/10.1146/annurev.immunol.021908.132620.
18. Libby P, Pasterkamp G, Crea F, Jang IK. Reassessing the mechanisms of acute coronary syndromes. Circ Res. 2019;124(1):150–60. https://doi.org/10.1161/CIRCRESAHA.118.311098.
19. Reimann C, Brangsch J, Colletini F, Walter T, Hamm B, Botnar RM, et al. Molecular imaging of the extracellular matrix in the context of atherosclerosis. Adv Drug Deliv Rev. 2017;113:49–60. https://doi.org/10.1016/j.addr.2016.09.005.
20. Sinha A, Shaporev A, Nosoudi N, Lei Y, Vertegel A, Lessner S, et al. Nanoparticle targeting to diseased vasculature for imaging and therapy. Nanomedicine. 2014;10(5):1003–12. https://doi.org/10.1016/j.nano.2014.02.002.
21. Perez-Medina C, Binderup T, Lobatto ME, Tang J, Calcagno C, Giesen L, et al. In vivo PET imaging of HDL in multiple atherosclerosis models. JACC Cardiovasc Imaging. 2016;9(8):950–61. https://doi.org/10.1016/j.jcmg.2016.01.020.
22. Caravan P, Das B, Dumas S, Epstein FH, Helm PA, Jacques V, et al. Collagen-targeted MRI contrast agent for molecular imaging of fibrosis. Angew Chem Int Ed Eng. 2007;46(43):8171–3. https://doi.org/10.1002/anie.200700700.
23. Kaspar M, Zardi L, Neri D. Fibronectin as target for tumor therapy. Int J Cancer. 2006;118(6):1331–9. https://doi.org/10.1002/ijc.21677.
24. Matter CM, Schuler PK, Alessi P, Meier P, Ricci R, Zhang D, et al. Molecular imaging of atherosclerotic plaques using a human antibody against the extra-domain B of fibronectin. Circ Res. 2004;95(12):1225–33. https://doi.org/10.1161/01.RES.0000150373.15149.ff.
25. Dietrich T, Berndorff D, Heinrich T, Hucko T, Stepina E, Hauff P, et al. Targeted ED-B fibronectin SPECT in vivo imaging in experimental atherosclerosis. Q J Nucl Med Mol Imaging. 2015;59(2):228–37.
26. Kim H, Lee Y, Kang S, Choi M, Lee S, Kim S, et al. Self-assembled nanoparticles comprising aptide-SN38 conjugates for use in targeted cancer therapy. Nanotechnology. 2016;27(48):48LT01. https://doi.org/10.1088/0957-4484/27/48/48LT01.
27. Starmans LW, van Duijnhoven SM, Rossin R, Aime S, Daemen MJ, Nicolay K, et al. SPECT imaging of fibrin using fibrin-binding peptides. Contrast Media Mol Imaging. 2013;8(3):229–37. https://doi.org/10.1002/cmmi.1521.
28. Starmans LW, van Duijnhoven SM, Rossin R, Berben M, Aime S, Daemen MJ, et al. Evaluation of 111In-labeled EPep and FibPep as tracers for fibrin SPECT imaging. Mol Pharm. 2013;10(11):4309–21. https://doi.org/10.1021/mp400406x.
29. Starmans LW, Moonen RP, Aussems-Custers E, Daemen MJ, Strijkers GJ, Nicolay K, et al. Evaluation of iron oxide nanoparticle micelles for magnetic particle imaging (MPI) of thrombosis. PLoS One. 2015;10(3):e0119257. https://doi.org/10.1371/journal.pone.0119257.
30. Yoo SP, Pineda F, Barrett JC, Poon C, Tirrell M, Chung EJ. Gadolinium-functionalized peptide amphiphile micelles for multimodal imaging of atherosclerotic lesions. ACS Omega. 2016;1(5):996–1003. https://doi.org/10.1021/acsomega.6b00210.
31. Simberg D, Duza T, Park JH, Essler M, Pilch J, Zhang L, et al. Biomimetic amplification of nanoparticle homing to tumors. Proc Natl Acad Sci U S A. 2007;104(3):932–6. https://doi.org/10.1073/pnas.0610298104.
32. Nahrendorf M, Jaffer FA, Kelly KA, Sosnovik DE, Aikawa E, Libby P, et al. Noninvasive vascular cell adhesion molecule-1 imaging identifies inflammatory activation of cells in atherosclerosis. Circulation. 2006;114(14):1504–11. https://doi.org/10.1161/CIRCULATIONAHA.106.646380.
33. Nahrendorf M, Keliher E, Panizzi P, Zhang H, Hembrador S, Figueiredo JL, et al. 18F-4V for PET-CT imaging of VCAM-1 expression in atherosclerosis. JACC Cardiovasc Imaging. 2009;2(10):1213–22. https://doi.org/10.1016/j.jcmg.2009.04.016.
34. McAteer MA, Schneider JE, Ali ZA, Warrick N, Bursill CA, von zur Muhlen C, et al. Magnetic resonance imaging of endothelial adhesion molecules in mouse atherosclerosis using dual-targeted microparticles of iron oxide. Arterioscler Thromb Vasc Biol. 2008;28(1):77–83. https://doi.org/10.1161/ATVBAHA.107.145466.
35. Stein-Merlob AF, Hara T, McCarthy JR, Mauskapf A, Hamilton JA, Ntziachristos V, et al. Atheroma susceptible to thrombosis exhibit impaired endothelial permeability in vivo as assessed by nanoparticle-based fluorescence molecular imaging. Circ Cardiovasc Imaging 2017;10(5) doi:https://doi.org/10.1161/CIRCIMAGING.116.005813.
36. Wang Y, Chen J, Yang B, Qiao H, Gao L, Su T, et al. In vivo MR and fluorescence dual-modality imaging of atherosclerosis characteristics in mice using profilin-1 targeted magnetic nanoparticles. Theranostics. 2016;6(2):272–86. https://doi.org/10.7150/thno.13350.
37. Grootaert MOJ, Moulis M, Roth L, Martinet W, Vindis C, Bennett MR, et al. Vascular smooth muscle cell death, autophagy and

senescence in atherosclerosis. Cardiovasc Res. 2018;114(4):622–34. https://doi.org/10.1093/cvr/cvy007.
38. Winkels H, Ehinger E, Ghosheh Y, Wolf D, Ley K. Atherosclerosis in the single-cell era. Curr Opin Lipidol. 2018;29(5):389–96. https://doi.org/10.1097/MOL.0000000000000537.
39. Winkels H, Ehinger E, Vassallo M, Buscher K, Dinh HQ, Kobiyama K, et al. Atlas of the immune cell repertoire in mouse atherosclerosis defined by single-cell RNA-sequencing and mass cytometry. Circ Res. 2018;122(12):1675–88. https://doi.org/10.1161/CIRCRESAHA.117.312513.
40. Cochain C, Vafadarnejad E, Arampatzi P, Pelisek J, Winkels H, Ley K, et al. Single-cell RNA-seq reveals the transcriptional landscape and heterogeneity of aortic macrophages in murine atherosclerosis. Circ Res. 2018;122(12):1661–74. https://doi.org/10.1161/CIRCRESAHA.117.312509.
41. Cole JE, Park I, Ahern DJ, Kassiteridi C, Danso Abeam D, Goddard ME, et al. Immune cell census in murine atherosclerosis: cytometry by time of flight illuminates vascular myeloid cell diversity. Cardiovasc Res. 2018;114(10):1360–71. https://doi.org/10.1093/cvr/cvy109.
42. Konopka CJ, Wozniak M, Hedhli J, Ploska A, Schwartz-Duval A, Siekierzycka A, et al. Multimodal imaging of the receptor for advanced glycation end-products with molecularly targeted nanoparticles. Theranostics. 2018;8(18):5012–24. https://doi.org/10.7150/thno.24791.
43. Majmudar MD, Yoo J, Keliher EJ, Truelove JJ, Iwamoto Y, Sena B, et al. Polymeric nanoparticle PET/MR imaging allows macrophage detection in atherosclerotic plaques. Circ Res. 2013;112(5):755–61. https://doi.org/10.1161/CIRCRESAHA.111.300576.
44. Keliher EJ, Ye YX, Wojtkiewicz GR, Aguirre AD, Tricot B, Senders ML, et al. Polyglucose nanoparticles with renal elimination and macrophage avidity facilitate PET imaging in ischaemic heart disease. Nat Commun. 2017;8:14064. https://doi.org/10.1038/ncomms14064.
45. Lee JM, Choudhury RP. Atherosclerosis regression and high-density lipoproteins. Expert Rev Cardiovasc Ther. 2010;8(9):1325–34. https://doi.org/10.1586/erc.10.108.
46. Brown WV, Brewer HB, Rader DJ, Schaefer EJ. HDL as a treatment target. J Clin Lipidol. 2010;4(1):5–16. https://doi.org/10.1016/j.jacl.2009.12.005.
47. Karalis I, Jukema JW. HDL mimetics infusion and regression of atherosclerosis: is it still considered a valid therapeutic option? Curr Cardiol Rep. 2018;20(8):66. https://doi.org/10.1007/s11886-018-1004-9.
48. Mulder WJM, van Leent MMT, Lameijer M, Fisher EA, Fayad ZA, Perez-Medina C. High-density lipoprotein nanobiologics for precision medicine. Acc Chem Res. 2018;51(1):127–37. https://doi.org/10.1021/acs.accounts.7b00339.
49. Zheng KH, van der Valk FM, Smits LP, Sandberg M, Dasseux JL, Baron R, et al. HDL mimetic CER-001 targets atherosclerotic plaques in patients. Atherosclerosis. 2016;251:381–8. https://doi.org/10.1016/j.atherosclerosis.2016.05.038.
50. Tang J, Lobatto ME, Hassing L, van der Staay S, van Rijs SM, Calcagno C, et al. Inhibiting macrophage proliferation suppresses atherosclerotic plaque inflammation. Sci Adv. 2015;1(3):e1400223. https://doi.org/10.1126/sciadv.1400223.
51. Seijkens TTP, van Tiel CM, Kusters PJH, Atzler D, Soehnlein O, Zarzycka B, et al. Targeting CD40-induced TRAF6 signaling in macrophages reduces atherosclerosis. J Am Coll Cardiol. 2018;71(5):527–42. https://doi.org/10.1016/j.jacc.2017.11.055.
52. Wen S, Liu DF, Cui Y, Harris SS, Chen YC, Li KC, et al. In vivo MRI detection of carotid atherosclerotic lesions and kidney inflammation in ApoE-deficient mice by using LOX-1 targeted iron nanoparticles. Nanomedicine. 2014;10(3):639–49. https://doi.org/10.1016/j.nano.2013.09.009.
53. Mitra S, Goyal T, Mehta JL. Oxidized LDL, LOX-1 and atherosclerosis. Cardiovasc Drugs Ther. 2011;25(5):419–29. https://doi.org/10.1007/s10557-011-6341-5.
54. Nie S, Zhang J, Martinez-Zaguilan R, Sennoune S, Hossen MN, Lichtenstein AH, et al. Detection of atherosclerotic lesions and intimal macrophages using CD36-targeted nanovesicles. J Control Release. 2015;220(Pt A):61–70. https://doi.org/10.1016/j.jconrel.2015.10.004.
55. Tarin C, Carril M, Martin-Ventura JL, Markuerkiaga I, Padro D, Llamas-Granda P, et al. Targeted gold-coated iron oxide nanoparticles for CD163 detection in atherosclerosis by MRI. Sci Rep. 2015;5:17135. https://doi.org/10.1038/srep17135.
56. Beldman TJ, Senders ML, Alaarg A, Perez-Medina C, Tang J, Zhao Y, et al. Hyaluronan nanoparticles selectively target plaque-associated macrophages and improve plaque stability in atherosclerosis. ACS Nano. 2017;11(6):5785–99. https://doi.org/10.1021/acsnano.7b01385.
57. Luehmann HP, Detering L, Fors BP, Pressly ED, Woodard PK, Randolph GJ, et al. PET/CT imaging of chemokine receptors in inflammatory atherosclerosis using targeted nanoparticles. J Nucl Med. 2016;57(7):1124–9. https://doi.org/10.2967/jnumed.115.166751.
58. Bagalkot V, Deiuliis JA, Rajagopalan S, Maiseyeu A. "Eat me" imaging and therapy. Adv Drug Deliv Rev. 2016;99(**Pt A**:2–11. https://doi.org/10.1016/j.addr.2016.01.009.
59. Poh S, Putt KS, Low PS. Folate-targeted dendrimers selectively accumulate at sites of inflammation in mouse models of ulcerative colitis and atherosclerosis. Biomacromolecules. 2017;18(10):3082–8. https://doi.org/10.1021/acs.biomac.7b00728.
60. Moreno-Layseca P, Icha J, Hamidi H, Ivaska J. Integrin trafficking in cells and tissues. Nat Cell Biol. 2019;21:122–32. https://doi.org/10.1038/s41556-018-0223-z.
61. Chen CL, Siow TY, Chou CH, Lin CH, Lin MH, Chen YC, et al. Targeted superparamagnetic iron oxide nanoparticles for in vivo magnetic resonance imaging of T-cells in rheumatoid arthritis. Mol Imaging Biol. 2017;19(2):233–44. https://doi.org/10.1007/s11307-016-1001-6.
62. Capolla S, Garrovo C, Zorzet S, Lorenzon A, Rampazzo E, Spretz R, et al. Targeted tumor imaging of anti-CD20-polymeric nanoparticles developed for the diagnosis of B-cell malignancies. Int J Nanomedicine. 2015;10:4099–109. https://doi.org/10.2147/IJN.S78995.
63. Naruko T, Ueda M, Haze K, van der Wal AC, van der Loos CM, Itoh A, et al. Neutrophil infiltration of culprit lesions in acute coronary syndromes. Circulation. 2002;106(23):2894–900.
64. Doring Y, Soehnlein O, Weber C. Neutrophil extracellular traps in atherosclerosis and atherothrombosis. Circ Res. 2017;120(4):736–43. https://doi.org/10.1161/CIRCRESAHA.116.309692.
65. Pertiwi KR, van der Wal AC, Pabittei DR, Mackaaij C, van Leeuwen MB, Li X, et al. Neutrophil extracellular traps participate in all different types of thrombotic and haemorrhagic complications of coronary atherosclerosis. Thromb Haemost. 2018;118(6):1078–87. https://doi.org/10.1055/s-0038-1641749.
66. Brinkmann V, Reichard U, Goosmann C, Fauler B, Uhlemann Y, Weiss DS, et al. Neutrophil extracellular traps kill bacteria. Science. 2004;303(5663):1532–5. https://doi.org/10.1126/science.1092385.
67. Pellico J, Lechuga-Vieco AV, Almarza E, Hidalgo A, Mesa-Nunez C, Fernandez-Barahona I, et al. In vivo imaging of lung inflammation with neutrophil-specific (68)Ga nano-radiotracer. Sci Rep. 2017;7(1):13242. https://doi.org/10.1038/s41598-017-12829-y.